# Rapid Water Harvesting and Nonthermal Drying in Humid Air by **N-Doped Graphene Micropads**

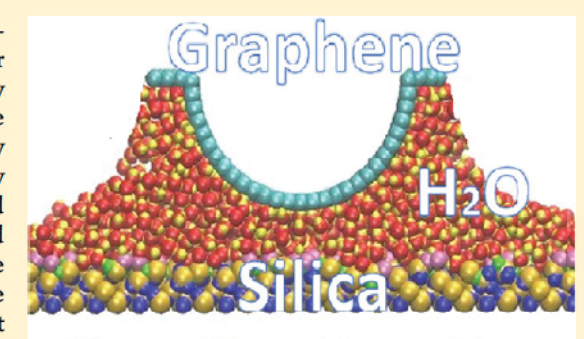
Yiyang Wan, †, § Dong Gao, †, ‡, § Jie Wang, †, ‡ Yanqing Yang, ‡ and Zhenhai Xia \*, †, ‡

Department of Materials Science and Engineering, and Department of Chemistry, University of North Texas, Denton, Texas 76203, United States

\*School of Materials Science and Engineering, Northwestern Polytechnical University, Xi'an, Shaanxi 710072, P. R. China

Supporting Information

ABSTRACT: We demonstrate a novel nanotextured graphene micropad that can rapidly harvest water from air to generate microscale water droplets with the desired size in designated positions on demand by simply applying a negative electric bias of -1.5 to -15 V. More interestingly, the water droplets can be reversibly dried nonthermally with the pad at ambient temperature in humid air (~85% RH) by applying a positive electric bias of +1.5 to +15 V. The harvesting and drying rates on the glass are 2.7 and 1.5  $\mu$ m<sup>3</sup>/s under biases of –15 and +15 V, respectively, but no apparent harvesting or drying activities are observed without the bias. The energy consumption is minimal as there is no Joule current due to the insulative substrate. It is shown that substrate wettability and ions play an important role in enabling the fast water harvesting and nonthermal drying. Molecular modeling is developed to understand the harvesting and drying mechanisms at



## Vapor Water Harvesting

the atomic scale. The water harvesting/drying approach may be useful for many technological applications such as micro/ nanolithography, 3D printing, MEMS, and biochemical and microfluid devices.

#### 1. INTRODUCTION

Water cycling from vapor water harvesting to drying is an essential part of our daily lives and is useful for technological applications such as environmental controls, food production, and medical treatments. In particular, being able to effectively control the micro-objects renders them appealing for many applications such as surface chemistry, micro/nanolithogra-phy, nanofabrication, MEMS, and biochemical and microfluid 9-12 devices. Traditional solutions to generating water in micro/nanoscale need complex design of water channels and controllers. <sup>13-15</sup> An alternative approach is to directly control the water liquid/gas status by water harvesting from air and water evaporation to air. In nature, some species, such as Namib Desert beetles<sup>16</sup> and spider silks,<sup>17</sup> have the ability to harvest water from dew or fog. Many bioinspired waterharvesting devices have been developed by fabricating hydrophobic-hydrophilic structures or periodic spindle-knots. 18,19 Apart from water collection, water removal from surfaces is also principal for microscale water management. The water can be dried through evaporation, electrolysis, and chemical reaction. Among them, chemical reaction and electrolysis are not suitable in microsystems due to the additional electrodes, reactors, or products. While thermal evaporation is simple, it is challenging to target a single water droplet on substrates in the microscale.

In the microscale, atomic force microscopy (AFM) has been used to form small water bridges from air when electric bias was applied.<sup>20</sup> However, the substrates needed to generate water

from air are conductive in most case. Here, we demonstrated that the nanotextured graphene surface showed rapid waterharvesting capability on insulative substrates (glass, mica, etc.) under a negative bias. In addition, the collected water droplets can be reversibly and quickly dried out at ambient temperature in highly humid air by applying a positive electric bias. This reversible water management could be applied in water harvesting, defogging, microsystem controlling, micro/nanofabrication, and microrobotics, to name a few.

#### 2. METHODS

2.1. Preparing Micropads on Tipless AFM Probes. Tipless AFM probes with a length of 225 µm (Forta-TL, AppNano) were selected as cantilevers. N-doped graphene, Teflon (PTFE tape, Harvey Inc.), LDPE thin films (Cling Wrap, Glad Inc.), and aluminum foils (Reynolds Inc.) were compressed in a compress machine and cut into small pads with a suitable size ( $\sim 30 \times 30 \,\mu\text{m}$ ) under the microscope or with focused ion beam (FIB). Four probes were made for each pad material and were randomly selected in the experiments. The wetting angles of N-doped graphene, Teflon, LDPE, and aluminum were measured to be >85, 133.7, 55.9, and  $86.9^{\circ}$ , respectively.  $^{20}$  The pads were glued to the end of cantilevers by epoxy glue (30 min slow-cure epoxy, Kite Studio Co., Inc.). Probes were then installed to atomic force microscopy (Dimension-Icon AFM, Bruker Co., Inc.) for water

Received: June 18, 2019 August 25, 2019 Published: September 1, 2019



harvesting and drying experiments. Individual cables were connected to the probe holder and the sample holder, which were connected to a wave generator.

**2.2.** Water Harvesting and Drying. Tipless AFM probes (Forta-TL, AppNano) glued with graphene pads were used in water harvesting and drying experiments. The spring constant of the probes is between 1.1 and 2.1 N/m. Glass slides (Fisherbrand, Fisher Scientific Co., Inc.), mica, and sapphire substrates (Bruker Co., Inc.) were dried for 24 h. The wetting angles of glass slide, mica, and sapphire substrate were measured to be 41.4, 10.2, and 79.5°, respectively. The experimental setup is illustrated in Figure 1A. The AFM chamber was filled with

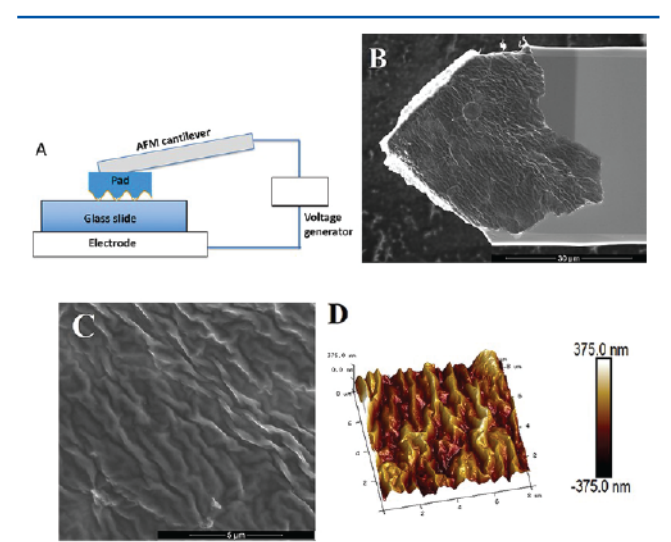


Figure 1. An overview of AFM testing system and nanoconvex graphene surface. (A) Schematic of experimental setup of water harvesting and drying using AFM under electric bias. (B) Image of AFM cantilever glued with graphene micropad. (C) Image of graphene with nanoscale concave—convex texture, which resembles topological structures of the textured surface of the depressed areas on Stenocara overwing of Namib Desert beetle forewing structures. <sup>16</sup> (D) AFM image of three-dimensional topological surface structure of the graphene on AFM tip.

mixed air and steam to reach certain RH in the chamber, and the RH was then maintained for 1 h at room temperature (22 °C) before any test was made. The probe with graphene pads was installed, and the substrates were placed on the conductive holder. In water vapor collection, negative bias was applied on the cantilever, and the cantilever was then engaged to the substrate surface and maintained contact with the substrate. After making contact with the substrate for a certain time, the cantilever was withdrawn from it, and the waterdrop diameters were measured and recorded as the initial diameter. Since the generated water may still remain partially on the pad, three to five contacts without bias were conducted on clean places to calculate the total water volume on both substrates and graphene pads.

In the water evaporation experiment, waterdrops of a certain size were produced with the water harvesting method. Positive bias was applied to the cantilever with the graphene pad, and the pad was engaged to or near the water droplets. During the drying, the pad was withdrawn and reengaged by several times for size measurement of the remaining water droplet. For each set of parameters, we made three trials with every probe. From the top view, the diameters of the water droplets were measured, and then the volumes of water droplets were calculated based on the model of spherical cap. With known cap diameter and wetting angle of the substrates, we calculated the volume by  $V = \frac{\pi}{3} r^3 (2 + \cos\theta) (1 - \cos\theta)^2$  in which r is the radius and  $\theta$  is the wetting angle. The standard deviations were calculated based on 12 trials in total for each data point. Because the collected waterdrops were not circular sometimes, the diameters were only measured along the horizontal direction no matter what shapes they were. As a result, the

errors were larger with increasing diameters of water and so was it for water volumes.

2.3. Modeling of Water Vapor Collection. The models for water harvesting are three-dimensional unit cells consisting of a single graphene convex, SiO<sub>2</sub> substrate saturated with silanol groups, and water molecules between them. The lateral size of the substrate plates is 50-200 Å, with a thickness of 15-20 Å. The height of the model is kept large ( $\sim$ 100 Å), and a number of water molecules were placed in the gap between the substrate and graphene. To simulate the effect of applied electric field, positive (or negative) electric charges equivalent to the applied electric bias were distributed uniformly on the graphene convex. The bonded interactions for SiO<sub>2</sub> and graphene are described by Tersoff potential<sup>21</sup> and modified AIRBO potential,<sup>22</sup> respectively. For silanol groups on the surface of SiO2, the bonded energies including contributions from bonds and angles of Si-O-H were described by force field potential, and nonbonded interactions were taken as the sum of van der Waals (Lennard-Jones) and electrostatic point charge potentials centered on the atoms. Water molecules were modeled by the three-site models (TIP3P).<sup>23</sup> The parameters for the force field potential and nonbonded interactions were described in details.<sup>20</sup> long-range interactions were computed using the particle-particle particle-mesh (PPPM) algorithm in reciprocal space. Periodic boundary conditions were imposed in x and y directions. MD simulations were performed using LAMMPS with a time step of 0.5 fs for the velocity Verlet integrator. <sup>24</sup> The system was equilibrated at 300 K for 1 ns. All the runs were in the NVT ensemble with the temperature controlled by a Nose-Hoover thermostat with a 100 fs damping parameter.

#### 3. RESULTS

3.1. Water Harvesting from Humid Air. Water harvesting from humid air was carried out in an AFM system (Figure 1A). AFM tipless probes glued with N-doped graphene flakes (Figure 1B) were used to collect water. The N-doped graphene (~5 layers) was fabricated with chemical vapor deposition (CVD) method.<sup>25</sup> After it was doped with nitrogen, the graphene became wrinkled, with a nanoscale concave-convex texture (Figure 1C,D). This nanoconcave—convex structure could form alternative hydrophobic and hydrophilic areas due to the tip effect under an applied electric potential, resembling Namib Desert beetle forewing structures, which promotes local wettability of chemical species such as water molecules.<sup>26</sup> Theoretical analysis shows that concave-convex structures are important in determining the wettability.  $^{31}$  An electric double layer (EDL) will also be formed on the surface of the graphene under an electric potential. In addition, wrinkled surface of graphene also provides a larger surface area to store more charges and attract water molecules.

We observed that a microscale water droplet was rapidly generated underneath the graphene pad when the pad contacts flat glass surface under a negative electric bias (Figure 2A and Movie S1). Although the growth of nanoscale water bridges between conductive AFM tip and conductive substrates was observed previously,<sup>30</sup> here in our experiment, the microscale water droplet was generated on an insulative substrate (glass) with a relatively low electric potential ( $\sim$ -10 V). In addition, there is no electric current flow in the system during the water harvesting, indicating that energy consumption is minimal. Figure 2B shows the water harvesting rate of the graphene pad as a function of time on different substrates. The diameter of the droplet is linearly proportional to the cubic root of time for all the substrates including glass, mica, and sapphire. But the harvesting rate (the slope of the lines) seems to associate with the substrate wettability. Among the substrate tested in the experiment, mica shows the highest water collecting rate,

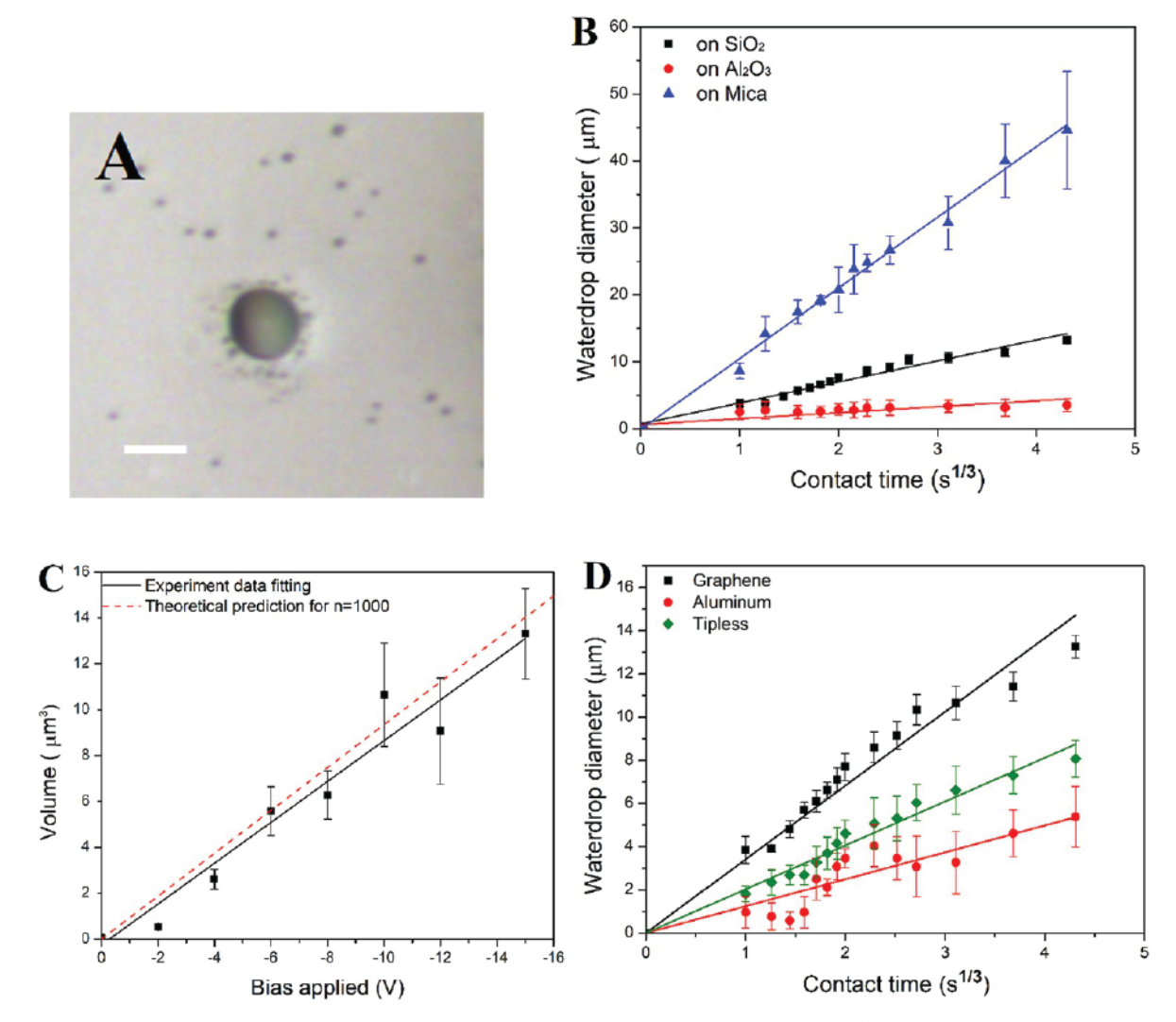


Figure 2. Water vapor harvesting of nanotextured graphene pads, driven by negative electric potential. (A) Water droplet grown on glass substrate in 10 min under a tip bias of -15 V (scale bar:  $20 \mu m$ ). (B) Size of water droplet growth on glass substrate as a function of time under a tip bias of -10 V at 85% humidity, collected with graphene pad. (C) Harvesting volume of water droplets as a function of the graphene tip bias for a contact time of 5 s on glass slides at 85% humidity. The experimental results were fitted using eq 1 (red dotted line), which agrees well with the experimental results for  $\beta = 0.235 \mu m^3/Vs$ . (D) Water harvesting rate for different pad materials on glass substrates under a tip bias of -10 V.

corresponding to the smallest wetting angle (highly hydrophilic), but there is no visible waterdrop collected on the Teflon substrate with the highest wetting angle (highly hydrophobic). On the other hand, with increasing electric bias, the collected water volume increases linearly but there is a lower limit of bias (~-1.5 V) below which no apparent water harvesting activity was observed (Figure 2C). Therefore, both the bias and surface wetting properties play an important role in water harvesting. The amount of water collected by the pad also corresponds to the force between the pad and substrate. As shown in Figure 3A,B, the force curve at the tip—substrate separation point is sharp without a tail at the beginning of the water harvesting because of the van der Waals force in action only, but the tail becomes larger and larger in the retreating as the amount of collected water increases.

To gain more insight into the effect of the materials properties of the AFM pads, we selected three more materials, low-density polyethylene (LDPE), aluminum and Teflon thin films, for the harvesting experiment according to their surface properties (wetting angle,  $\theta$ ). Among these selected materials, Teflon and LDPE are insulative, but the former is the most hydrophobic ( $\theta$ )

= 133.7°) while the latter is the most hydrophilic ( $\theta = 55.9^{\circ}$ ). On contrast, aluminum is conductive, and its wetting angle is 86.9° below but close to  $90^{\circ}$ , similar to the graphene ( $\theta > 85^{\circ}$ ). For all the materials, the harvested water volume increases linearly with the time (Figure 2D). The graphene pad has the highest water harvesting rate on mica, while the insulative pads (Teflon and LDPE) do not have the capability to harvest water at all. The excellent harvesting capability of the graphene pads may be attributed to the unique concave—convex structure and larger surface area of the N-doped graphene compared with the aluminum and tipless probe pads. The wrinkled area of graphene would be more attractive to water molecules and ions under an electric bias. Therefore, among the materials and structures tested in this experiment, the graphene stands out as the best materials probably owning to its unique nanoconcave—convex structures.

**3.2.** Nonthermal Drying of Water Droplets. While water vapor can be harvested rapidly by the textured graphene pads under negative bias, we also observed for the first time that the collected water droplets on substrates can be dried reversibly in highly humid air by simply applying positive electric bias on the

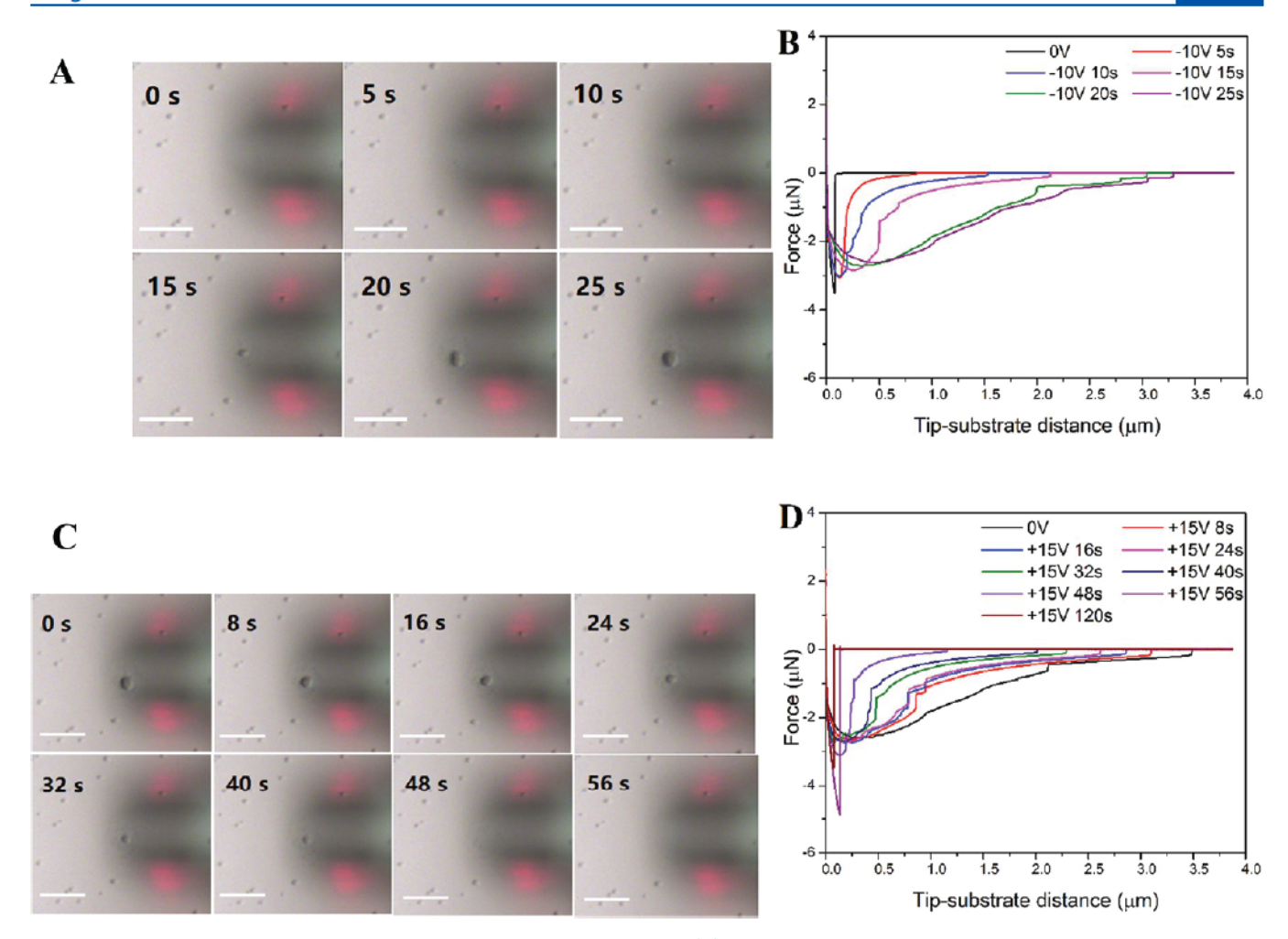


Figure 3. Relationship between droplet size and force during collecting/drying. (A) Photographs of a water droplet being generated under an applied bias of -10 V. (B) Force—distance curves measured during water collecting. (C) Photographs of a water droplet under an applied bias of +15 V. (D) Force—distance curves measured during water drying. Scale bars: 50  $\mu$ m.

graphene pads at room temperature (22 °C). The water drying process was shown by Movies (water vaporization under a positive electric bias, Movie S2). Figure 4A shows the drying rate as a function of time for a droplet underneath or near the pads with a distance from  $0-45 \mu m$  under an applied bias of +10 V at ~85% RH. A 10  $\mu$ m water droplet on the glass disappeared in just 30 s. Even a water droplet near the graphene pad can also be dried, as illustrated in Figure 4C, where the drying rate reduces with the distance from the pad (Figure 4B). Without the applied bias, there was no visible change in the size of the waterdrop as long as the humidity and temperature were maintained. The drying rate of the water depends on the electric bias and the distance from the pad to waterdrops. The amount of remaining water during the drying also corresponds to the force between the pad and substrate. The tail of force curves becomes smaller and smaller in the retreating of the AFM probe with reducing amount of water (Figure 3C,D). No tail was observed after drying because the van der Waals force dominates the process.

We have tested LDPE, aluminum, and Teflon thin films under the same conditions as well but only conductive AFM pads show water drying capability. It was reported that attoliter  $(10^{-18} \, \text{L})$  water droplet was evaporated with a tip bias of  $-10 \, \text{V}$  after 24 min.<sup>33</sup> The droplet evaporation in this case was caused by an ionic current and Joule heating induced by the bias applied on two conductive electrodes. However, in our experiment, again,

there is no apparent current flow because of the insulative substrate during the drying by the graphene pad. If there were current flow through ions, the water should have been heated up and vaporized during water harvesting under a negative bias because the heat is independent of the current direction. However, we observed the water removal by the positive bias as well as the water capture by the negative bias. Thus, no Joule heat is generated at the pad or substrate to heat up the droplet. This nonthermal drying process is not a natural drying because no apparent water drying activity was observed without the applied bias at ambient temperature. This unusual water drying ability provides an effective approach to enhance the evaporation of water into a nearly saturated humid atmosphere, preventing unwanted condensation in local area.

The water harvesting and drying processes can even be made repeatedly by alternatively turning the negative and positive biases, respectively, as shown in Movie S3. To directly observe the growth of water droplets at the microscale, we used a special silicon AFM tip, an elephant nose-like probe, to visualize the water harvesting—drying cycles at the tip. As shown in Figure 5, a drop of water with a diameter of  $\sim\!20\,\mu\mathrm{m}$  was generated at the tip under a bias of -15 V in 6 min. This waterdrop was dried in 3 h by applying +15 V bias, but it remained almost unchanged without the applied bias. Such a water management is useful in

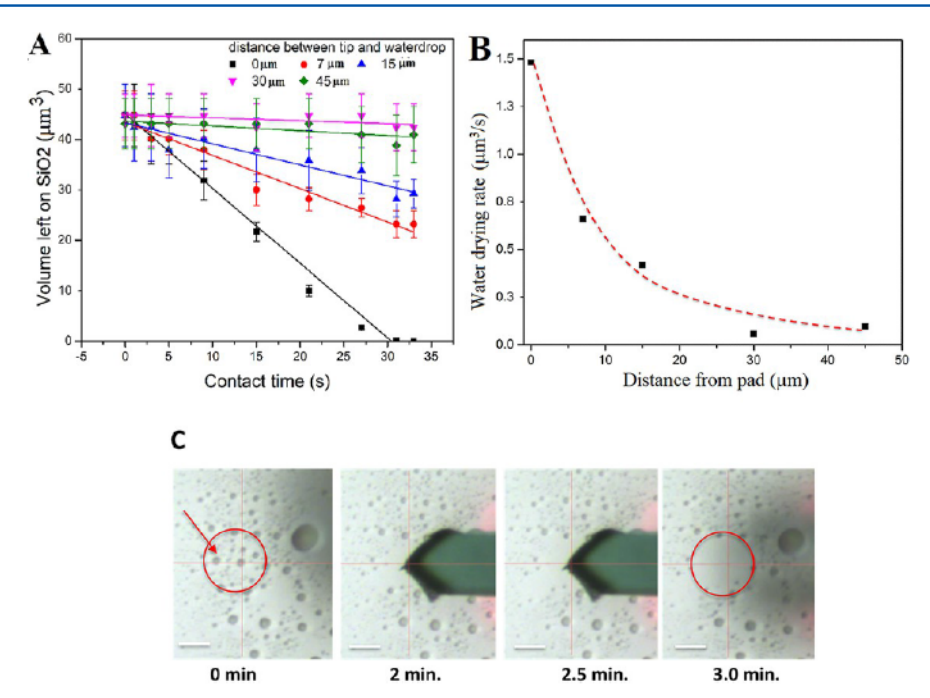


Figure 4. Water drying by graphene pads, driven by positive electric potential. (A) Water evaporation volume as a function of time at 85% RH. (B) Water evaporation rate as a function of the distance from the pad (red dotted curve: fitting curve). All the experiments were done at 85% RH and ambient temperature. (C) Photographs (scale bar,  $15 \mu m$ ) of water drying near and under the graphene pad at different times, under an applied bias of +10 V. Before the pad made contact with the substrate, there were water droplets on the surface of the substrate. After  $\sim$ 3 min, all the droplets disappeared in the area marked by red circle. Even the droplets near the pad (arrow) rapidly evaporated.

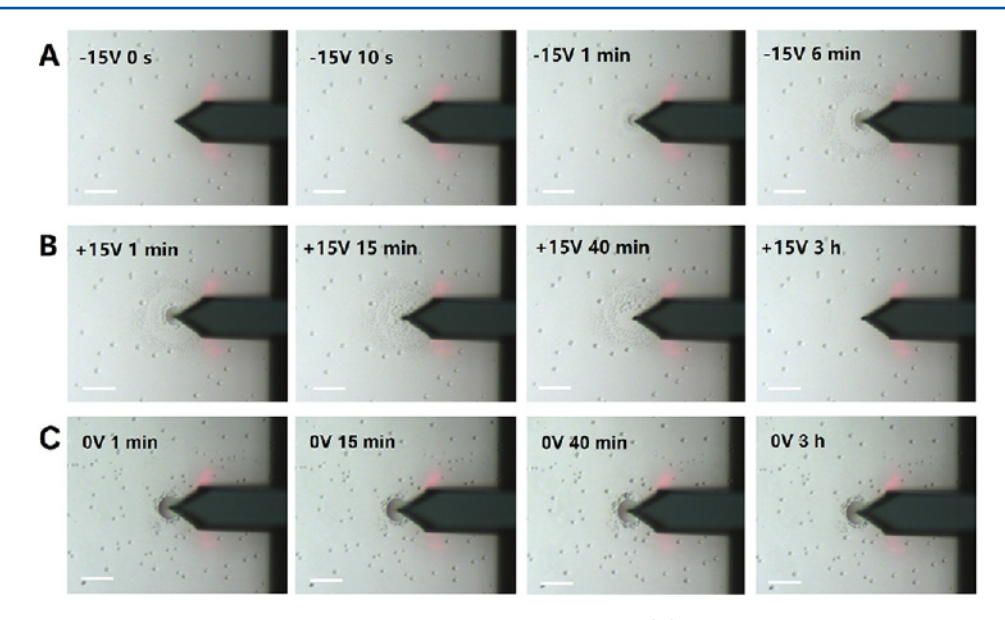


Figure 5. Water droplets during the collection/drying with elephant nose-like tip on glass. (A) Four upper row pictures of water droplet growing at the tip under a bias of -15 V at 85% RH. (B) Four lower row pictures of water droplet drying at the tip under a bias of +15 V at 85% RH. Scale bars:  $50 \mu m$ . (C) Water droplet without bias at 85% RH.

controlling micro-objects for many technological implementations.

**3.3.** Water Harvesting/Drying Mechanisms. To understand the mechanism of the unusual water harvesting and drying, we conducted more experiments on the substrate under different conditions. First, we put the graphene pad near a water droplet on the mica surface under a given bias and observed that the water droplets were sucked toward the pad and dried out in a couple of minutes (Figure 6). This experiment indicates that the graphene pad also collects the water from the

surface of the substrates. Second, we built a ring barrier on glass slides with the epoxy glue that has similar wetting angle as glass slides (Figure 7A). The ring barrier is about  $10 \,\mu m$  in height and thus prevents the water outside the ring from moving across it. A top visual AFM probe (elephant nose-like probe, VIT\_P, NT-MDT Inc.) was engaged inside the ring for 1 h with a -15 V bias on, and a small waterdrop was observed (Figure 7B), but the same amount of water was collected in just 7 min outside of the ring (Figure 7C,D. The collection rate reduced significantly within the epoxy cage because of the inhibition of water

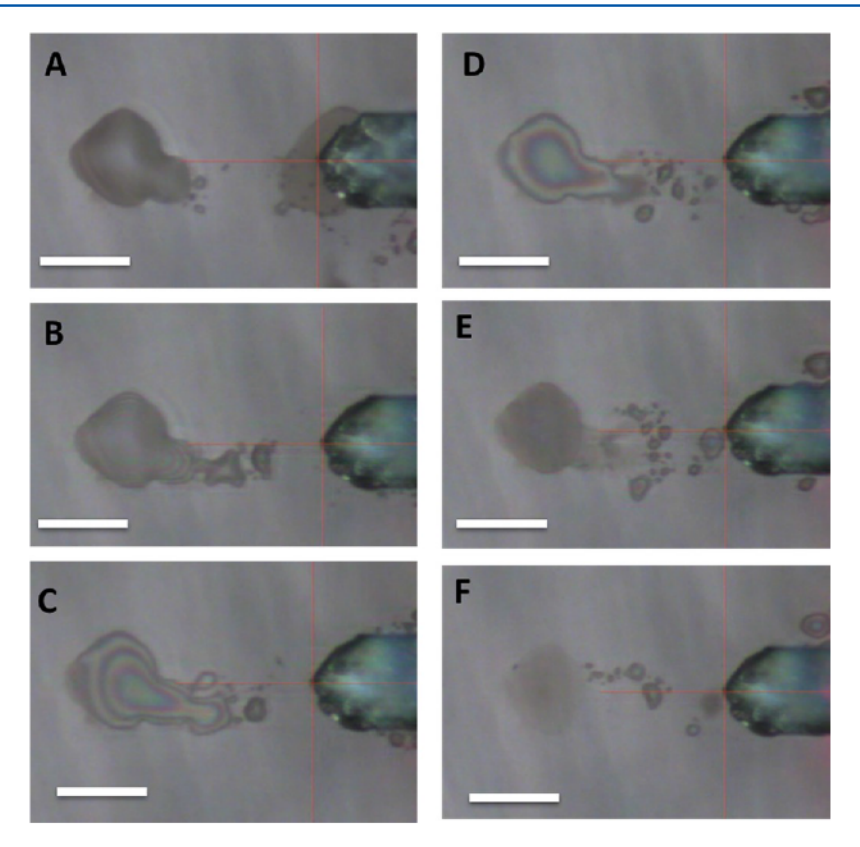


Figure 6. Optical images of transport process of water droplets on mica toward the pad at an electric bias of -10 V. The optical images (scale bar, 30  $\mu$ m) at (A) 0, (B) 2, (C) 4, (D) 6, (E) 8, and (F) 10 min after the bias was applied. At the beginning, only a small amount of water was collected at the AFM cantilever. After bias is on, waterdrops ( $\sim$ 25  $\mu$ m) near the cantilever were moving toward the cantilever, leaving water marks, and the end of cantilever was almost immerged in water. Finally, a large amount of water was left on the mica after the cantilever was retracted. The average loading force was 50 nN on the mica at 86% RH and 22 °C.

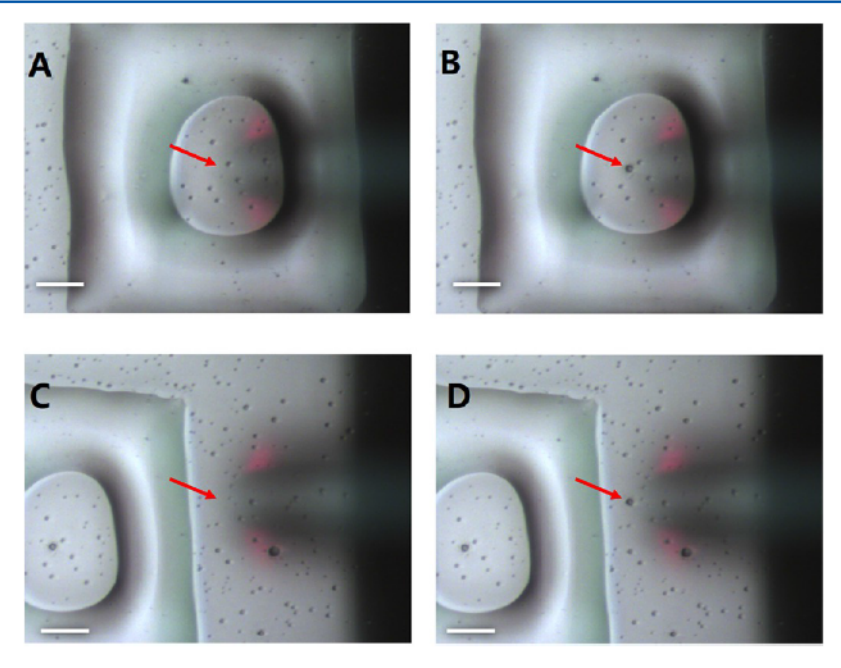


Figure 7. Water vapor harvesting of an elephant nose-like visual AFM tip inside/outside the epoxy ring barrier, driven by negative electric potential. (A) Inside of the epoxy ring barrier without the applied bias. (B) The water droplet generated inside of the epoxy ring barrier after 1 h under an applied bias of -10 V at RH of 85%. (C) No water droplet outside of the epoxy ring barrier at the beginning. (D) The water droplet generated outside of the epoxy ring barrier after 7 min under an applied bias of -10 V at RH of 85%.

movement on the glass surface. As a result, only water in air and on the limited surface could be attracted by the charged tip. A similar experiment was performed for water drying inside/ outside the cage. The drying rate outside the cage is much faster than that inside the cage, suggesting that water was pushed away along the surface and evaporated on a larger area surrounding

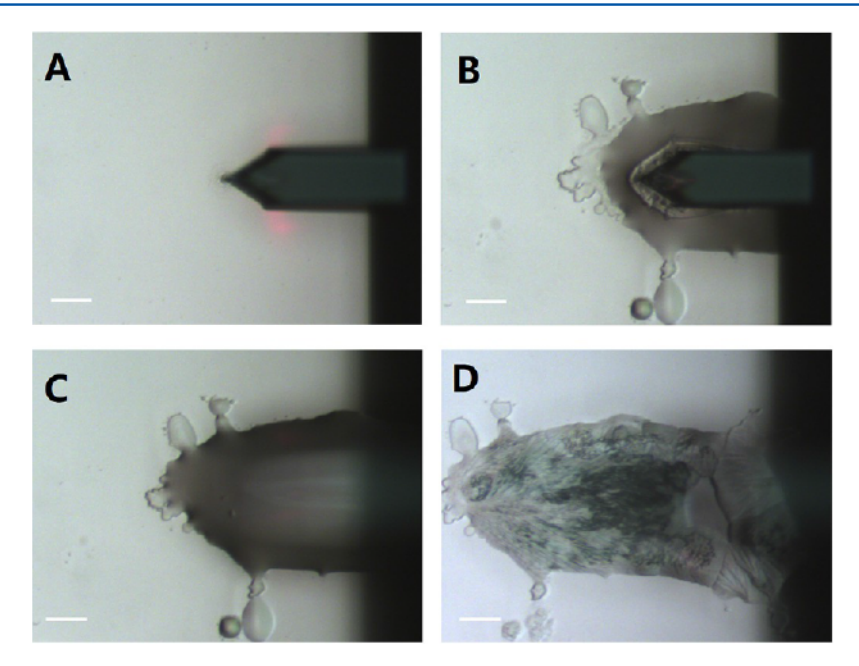


Figure 8. Water collection on the glass slide washed with 0.001 M NaHCO<sub>3</sub> solution. The water collected in (A) 10 s, (B) 16 h, and (C) 22 h, with an elephant nose-like tip at a bias of -15 V and a humidity of 85%. (D) NaHCO<sub>3</sub> crystal after the collected waterdrop was dried naturally at low RH.

the probe. Thus, substrates serve as a medium that significantly enhances both water harvesting and water drying processes.

We further investigated the role of ions in water harvesting and drying. We noticed that water collection hardly works on the glass slides that were cleaned with deionized water by an ultrasonicator. After immersing the cleaned slides into dilute solutions such as 0.001 M NaCl or NaHCO<sub>3</sub>, the AFM pad regain the water collection ability. Moreover, visible solute crystallization was observed after a long period (16 h) of water collection if the glass slide was treated by the dilute solutions (Figure 8). A similar phenomenon occurred on unwashed glass slides as well. On the other hand, the waterdrops on the retreated glass slides can be dried, and NaHCO<sub>3</sub> crystal was observed after drying (Figure 8D). Therefore, the solute or ions on the substrate played a considerable role in water harvesting and drying.

3.4. Molecular Modeling of Water Harvesting. It is well known that electric double layer (EDL) on the surface of the substrate (e.g., SiO<sub>2</sub>) can be induced by the adsorbed water from humid air. 34,35 There usually are a number of water layers adsorbed on substrates, depending on the RH, and the first one to two water adlayers on mica show an ice-like structure with a typical thickness of  $\sim 3.7$  Å.<sup>36</sup> Similar structures have been reported for the case of water layers trapped between graphene and hydrophilic sapphire and  $SiO_{2}^{37,38}$  An EDL is formed with negatively charged substrate surface and positively charged water layer through the dissociation of silanol groups: SiOH  $\rightarrow$ SiO<sup>-</sup> + H<sup>+</sup>. <sup>39</sup> Thus, there are counterions in the diffuse layer of the EDL. When a negative bias is applied to the pad, a radial electric field parallel to the surface is established in the direction to the pad (Figure 9A). The negatively charged pad would drive the conterions that drag the water to flow toward the pad, harvesting water from the surface. In addition, if there are ions in the surface water layers, under the electric field, the cations would drive water toward the tip as they are better carrier than anions. The solute in collected water also reduces the vapor pressure according to Raoult's Law and Kelvin equation, which lowers the speed of water revaporation.<sup>40</sup> In addition to driving

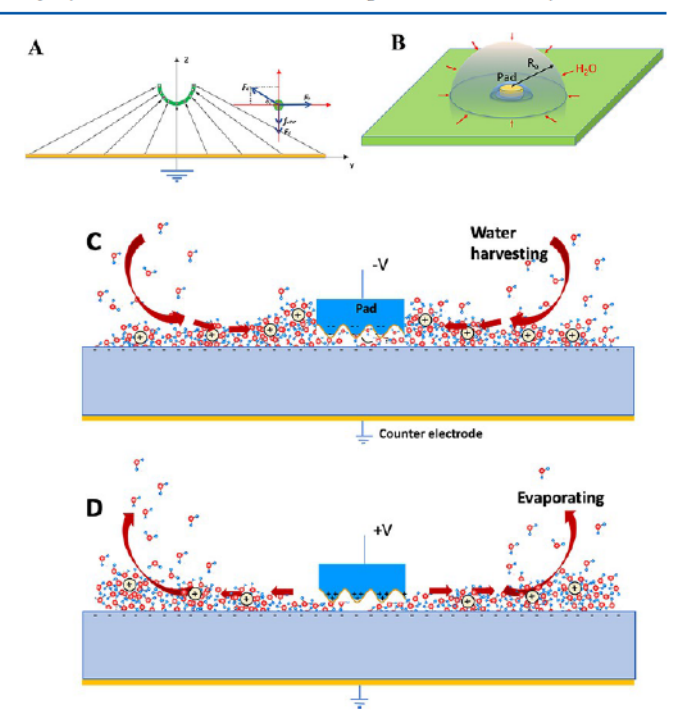


Figure 9. Schematics of effective electric field and fast water harvesting and drying. (A) Nonuniform electric field is generated by graphene pad in which water molecule (dipole) was pulled toward to the pad due to the electric field gradient. (B) Schematic of water harvesting system with an effective harvesting region  $(R_{\rm e})$ . Illustrations of (C) water harvesting mechanism and (D) water drying mechanism.

the surface water flow toward the pad, the applied electric field also reduces the vapor pressure. As a result, the water vapor in the effective distance of the electric field  $(R_e)$  would condense on the substrate surface (Figure 9B). Thus, depending on the magnitude of the electric field, the effective water-harvesting area would be much larger than the pad itself, making this water harvesting even more effective. As illustrated in Figure 9C, during this process, water vapor in air would continue

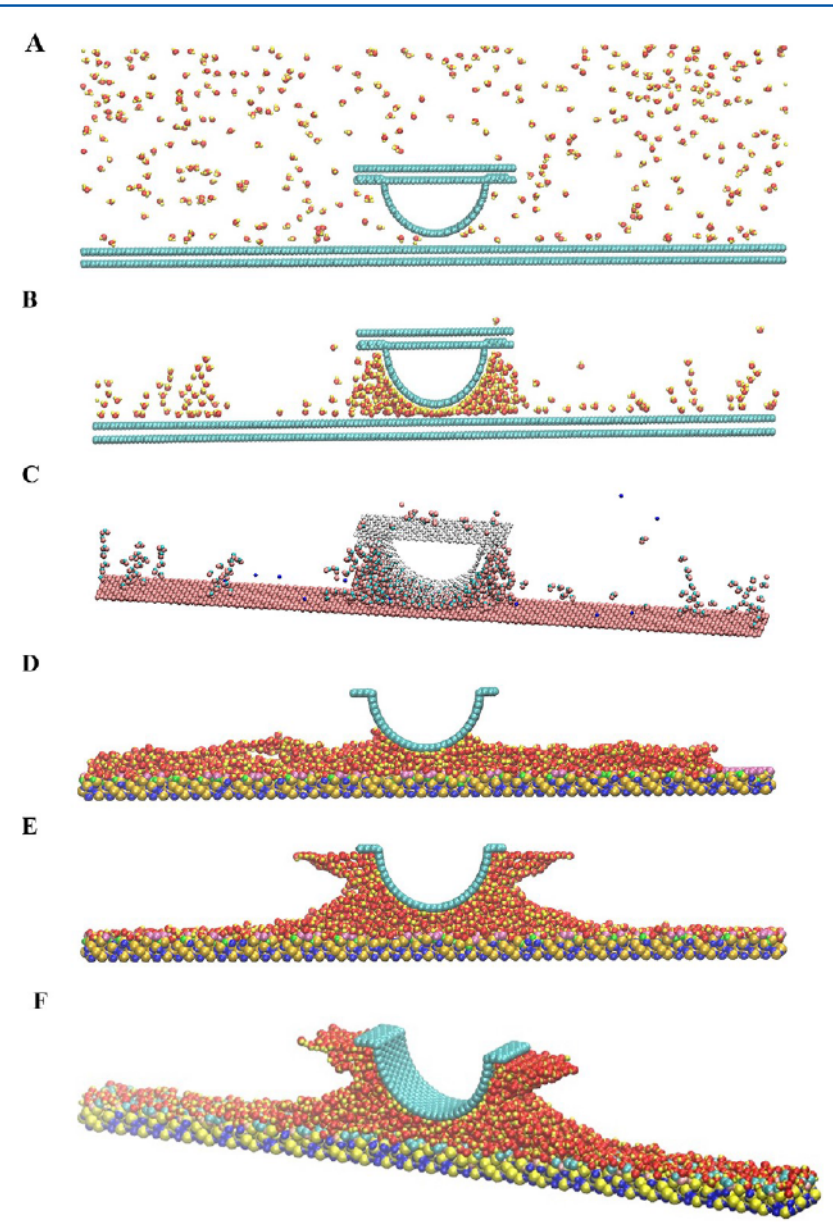


Figure 10. Snapshots of water harvesting from air using the graphene pad with nanoconcave—convex structure (A) before applying bias and (B) under a bias. Red, yellow, and blue balls refer to oxygen, hydrogen, and carbon (graphene) atoms, respectively. (C) 3D snapshots of water harvesting under a bias. Snapshots of vapor water harvesting from the  $SiO_2$  surface (D) before applying bias and (E) under a bias. Red, small yellow, blue, large yellow, and purple balls represent oxygen (water), hydrogen, carbon (graphene), silicon, and oxygen (substrate) atoms. (F) 3D snapshots of water harvesting under a bias on the  $SiO_2$  surface.

condensating on the surface area covered by the electric field, and the cations with condensed water were driven to flow toward the pad to form water droplets. Thus, the electric field significantly enhances the water condensation and accelerates harvesting speed by the surface effect.

The mechanisms of water harvesting were verified with MD simulations and its simulation procedure is described in Methods. As shown in Figure 10A–F, water molecules in air are pulled toward the pad. The water molecules far from the pad first condense to small droplets on the substrate surface and then flow toward the pad along the surface. With increasing electric bias, the effective area is enlarged, which accelerates the water harvesting rate.

The water harvesting rate is determined by a number of factors such as RH and applied bias. We assume that there is an effective radius  $R_{\rm e}$  (Figure 9B) within which ( $R < R_{\rm e}$ ) the water

molecules are accelerated to the pad due to the nonuniform electric field; but outside the region, the water molecule motion is controlled only by water diffusion in air or on the substrate surface. From fluid dynamics (Appendix A), the volume water harvesting rate  $(\nu)$  can be correlated with the applied voltage (U) and humidity  $(H_{\rm R})$  by

$$\nu = \beta H_{\rm R} U \tag{1}$$

where  $\beta$  is the constant related to the water diffusion coefficient, temperature, and system geometry. According to eq 1, the volume water harvesting rate is proportional to H<sub>R</sub> and U, which is in good agreement with our experimental results (Figure 2C).

The water drying capability is also attributed to the positively charged (counterion-containing) waterdrop collected from air and the substrate surface. When a positive bias is applied to the pad, the positively charged pad surface would push the cations

that drag water away from the graphene pad to the surrounding area, where water rapidly evaporates from the surface in a larger area, as illustrated in Figure 9D. With the enhanced effect, the pad and surrounding area are kept dry after a short period of time.

Overall, although according to Butt's work, <sup>41</sup> water is always driven to the electrode by electrical field, the ions in the droplets may play a dominant role in water harvesting and drying under electric field. The ions in the water or on the substrate surface serve as water couriers by forming ion—water complexes, promoting water transport. Under negative bias, the positive ions such as Na<sup>+</sup>, K<sup>+</sup>, and Mg<sup>2+</sup> on the glass would bring water to the negatively charged pads to harvest water. Under positive bias, the ions take water away from the positively charged pad. However, according to Butt et al., <sup>41</sup> pure water will be attracted to the probe no matter what the sign of bias is. Consequently, in the evaporation process, it has to overcome the condensation effect of water induced by the electric field. Thus, the overall drying rate with positive bias is always lower than the harvesting rate with negative bias, as observed in our experiment.

#### 4. CONCLUSIONS

In summary, we have achieved fast growth and evaporation of microscale water droplets on demand by designing the graphene surfaces with nanoconcave-convex texture, which are further enhanced and modulated by external stimuli (electric bias). Among the pad materials tested in this study, N-doped graphene stands out as the best one for water harvesting and drying in humid air at ambient temperature. To achieve the fast water harvesting and drying, the pad materials should be conductive and have large specific area while the substrate should have preexisting water layer on their surface or highly hydrophilic surface. The harvesting and drying rates increase with increasing the bias. Ions in the water play an important role in enhancing the water harvesting and drying. The rapid water droplet growth, combined with the ability of re-evaporation with the non-Joule effect, is crucial not only for water-harvesting and drying applications, particularly for heat-sensitive products, but also for many phase transfer applications. Because of no Joule heating, the energy consumption is minimal in the water harvesting and drying processes. We envision that this approach can be applied to a wide range of applications such as desalination, air conditioning, and distillation towers, to name a few.

## APPENDIX A

## Theoretical modeling of water harvesting

The applied electric field on the pad has effective distance  $R_{\rm e}$  beyond which water molecules in air are not affected by the field (Figure 9B). Thus, the water harvesting system can be divided into two regions, the inner region  $(R < R_{\rm e})$ , where water molecules are pulled toward the pad due to the dominant electrical potential energy (G) compared with thermal motion (namely,  $G > K_{\rm B}T$ ) leading to a velocity of water molecules toward the pad and the outer region  $(R > R_{\rm e})$ , where motion of water molecules is controlled by diffusion in air. Since the water molecules are accelerated toward the pad, there is a concentration gradient of the water molecules between the inner and outer regions, which determines the water harvesting rate. According to Fick's law, the diffusion flux (J) of water molecules from outer  $(R > R_{\rm e})$  to inner  $(R > R_{\rm e})$  region is given by

$$J = -D\frac{\partial c}{\partial R} \tag{A1}$$

where D and c are the diffusion coefficient (D, unit  $m^2$  s<sup>-1</sup>) and volume concentration of water molecules in air, respectively. Therefore, the mass of water accumulated from vapor in a certain time can be expressed by

$$m = JSt = D\frac{\partial c}{\partial r} 4\pi R_{\rm e}^2 t \tag{A2}$$

for simplicity, the concentration gradient can be approximated as

$$\frac{\partial c}{\partial R} = \alpha \frac{c}{R_{\rm e}} \tag{A3}$$

where  $\alpha$  is a factor. The volume concentration of vapor c can be related to humidities of air by

$$c = H_{\rm R}H_{\rm S} \tag{A4}$$

where  $H_{\rm R}$  and  $H_{\rm S}$  are the relative humidity (dimensionless quantity) and the saturated humidity in certain temperature and pressure, respectively. In addition, based on the equilibrium between electrical potential energy and thermal motion of water molecules ( $G = K_{\rm B}T$ ), we can obtain the effective radius.

$$R_{\rm e} = AQ^{1/2} \tag{A5}$$

where A is the constant related to temperature and Q is the charges on the convex surface of the convex-structured graphene, as mentioned above. Thus, the effective radius  $R_{\rm e}$  and electric bias U are related by

$$R_e = UA^2/K \tag{A6}$$

where K is the electrostatic constant. Combining eq A2-A6 yields the volume (V) of the water accumulated from vapor in a certain time (t).

$$V = \beta H_{\rm R} U t \tag{A7}$$

$$\beta = \frac{4\pi\alpha Dc^2 H_S}{\rho K} \tag{A8}$$

where  $\beta$  is a constant. Equation A7 establishes the relationship between the volume and time at a certain bias and/or relative humidity. According to eq A7, the harvested water volume is simply proportional to time (t), relative humidity  $(H_{\rm R})$ , and electric bias (U), which is in good agreement with our experimental results (Figure 2C).

### ASSOCIATED CONTENT

## Supporting Information

The Supporting Information is available free of charge on the ACS Publications website at DOI: 10.1021/acs.langmuir.9b01852.

Water harvesting under negative electric bias (MOV) Water drying under positive electric bias (MOV) Water harvesting—drying cycles (MOV)

## AUTHOR INFORMATION

## **Corresponding Author**

\*E-mail: Zhenhai.xia@unt.edu.

ORCID ®

Yiyang Wan: 0000-0002-8152-2892

Zhenhai Xia: 0000-0002-0881-2906

#### **Author Contributions**

§Y.W. and Y.G. contributed equally to this work.

#### Notes

The authors declare no competing financial interest.

#### ACKNOWLEDGMENTS

We thank the support from the National Science Foundation under the contract (1662288), Natural Science Foundation of China (51973174), and the Fundamental Research Funds for the Central Universities (3102019ZD0402). Computational resources were provided by UNT high-performance computing initiative.

## REFERENCES

- (1) Rykaczewski, K.; Scott, J. H. J. Methodology for imaging nano-to-microscale water condensation dynamics on complex nanostructures. *ACS Nano* 2011, 5, 5962–5968.
- (2) de La Rica, R.; Fabijanic, K. I.; Baldi, A.; Matsui, H. Biomimetic crystallization nanolithography: simultaneous nanopatterning and crystallization. *Angew. Chem., Int. Ed.* 2010, 49, 1447—1450.
- (3) Tseng, A. A. Advancements and challenges in development of atomic force microscopy for nanofabrication. *Nano Today* 2011, 6, 493-509.
- (4) Zheng, Y.; Han, D.; Zhai, J.; Jiang, L. In situinvestigation on dynamic suspending of microdroplet on lotus leaf and gradient of wettable micro- and nanostructure from water condensation. *Appl. Phys. Lett.* 2008, 92, 084106–1.
- (5) Ho, C.-H.; Tai, Y.-C. Micro-electro-mechanical-systems (MEMS) and fluid flows. *Annu. Rev. Fluid Mech.* 1998, 30, 579–612.
- (6) Unger, M. A.; Chou, H.-P.; Thorsen, T.; Scherer, A.; Quake, S. R. Monolithic microfabricated valves and pumps by multilayer soft lithography. *Science* **2000**, *288*, 113–116.
- (7) Chiou, P. Y.; Moon, H.; Toshiyoshi, H.; Kim, C.-J.; Wu, M. C. Light actuation of liquid by optoelectrowetting. *Sens. Acutators, A* 2003, 104, 222–228.
- (8) Meldrum, D. R.; Holl, M. R. Microscale bioanalytical systems. Science 2002, 297, 1197–1198.
- (9) Neale, S. L.; Macdonald, M. P.; Dholakia, K.; Krauss, T. F. Alloptical control of microfluidic components using form birefringence. *Nat. Mater.* 2005, 4, 530–533.
- (10) Cheng, L. J.; Chang, H. C. Microscale p H regulation by splitting water. *Biomicrofluidics* 2011, 5, 046502.
- (11) Liu, G. L.; Kim, J.; Lu, Y.; Lee, L. P. Optofluidic control using photothermal nanoparticles. *Nat. Mater.* 2006, 5, 27.
- (12) Martin, R. S.; Root, P. D.; Spence, D. M. Microfluidic technologies as platforms for performing quantitative cellular analyses in an in vitro environment. *Analyst* 2006, 131, 1197–1206.
- (13) Joanicot, M.; Ajdari, A. Droplet control for microfluidics. *Science* 2005, 309, 887–888.
- (14) Tan, Y. C.; Fisher, J. S.; Lee, A. I.; Cristini, V.; Lee, A. P. Design of microfluidic channel geometries for the control of droplet volume, chemical concentration, and sorting. *Lab Chip* 2004, *4*, 292–298.
- (15) Wu, J.; Zhang, M.; Li, X.; Wen, W. Multiple and high-throughput droplet reactions via combination of microsampling technique and microfluidic chip. *Anal. Chem.* 2012, 84, 9689–9693.
- (16) Parker, A. R.; Lawrence, C. R. Water capture by a desert beetle. *Nature* 2001, 414, 33–34.
- (17) Zheng, Y.; Bai, H.; Huang, Z.; Tian, X.; Nie, F.-Q.; Zhao, Y.; Zhai, J.; Jiang, L. Directional water collection on wetted spider silk. *Nature* 2010, 463, 640.
- (18) Zhu, H.; Guo, Z. Hybrid engineered materials with high water-collecting efficiency inspired by Namib Desert beetles. *Chem. Commun.* 2016, 52, 6809–6812.
- (19) Lee, S. H.; Lee, J. H.; Park, C. W.; Lee, C. Y.; Kim, K.; Tahk, D.; Kwak, M. K. Continuous fabrication of bio-inspired water collecting

surface via roll-type photolithography. Int. J. Precis. Eng. Manuf.-Green Technol. 2014, 1, 119-124.

- (20) Wan, Y.; Gao, Y.; Xia, Z. Highly Switchable Adhesion of N-Doped Graphene Interfaces for Robust Micromanipulation. *ACS Appl. Mater. Interfaces* 2019, 11, 5544–5553.
- (21) Munetoh, S.; Motooka, T.; Moriguchi, K.; Shintani, A. Interatomic potential for Si-O systems using Tersoff parameterization. *Comput. Mater. Sci.* 2007, 39, 334-339.
- (22) Brenner, D. W.; Shenderova, O. A.; Harrison, J. A.; Stuart, S. J.; Ni, B.; Sinnott, S. B. A second-generation reactive empirical bond order (REBO) potential energy expression for hydrocarbons. *J. Phys.: Condens. Matter* 2002, 14, 783–802.
- (23) Kim, J.; ChandrasekhaMhin, B. J.; Lee, S. J.; Kim, K. S. Entropydriven structures of the water octamer. *Chem. Phys. Lett.* 1994, 219, 243–246.
- (24) Plimpton, S. Fast parallel algorithms for short-range molecular dynamics. *J. Comput. Phys.* 1995, 117, 1–19 Supplementary.
- (25) Shao, Y.; Zhang, S.; Engelhard, M. H.; Li, G.; Shao, G.; Wang, Y.; Liu, J.; Aksay, I. A.; Lin, Y. Nitrogen-doped graphene and its electrochemical applications. *J. Mater. Chem.* 2010, 20, 7491–7496.
- (26) Xu, Q.; Wan, Y.; Hu, T. S.; Liu, T. X.; Tao, D.; Niewiarowski, P. H.; Tian, Y.; Liu, Y.; Dai, L.; Yang, Y.; Xia, Z. Robust self-cleaning and micromanipulation capabilities of gecko spatulae and their bio-mimics. *Nat. Commun.* 2015, *6*, 8949.
- (27) Li, W.; Li, Y.; Sheng, M.; Cui, S.; Wang, Z.; Zhang, X.; Yang, C.; Yu, Z.; Zhang, Y.; Tian, S.; Dai, Z.; Xu, Q. Enhanced Adhesion of Carbon Nanotubes by Dopamine Modification. *Langmuir* 2019, 35, 4527–4533.
- (28) Gómez-Moñivas, S.; Sáenz, J. J.; Calleja, M.; García, R. Field-induced formation of nanometer-sized water bridges. *Phys. Rev. Lett.* 2003, 91, No. 056101.
- (29) Cramer, T.; Zerbetto, F.; García, R. Molecular mechanism of water bridge buildup: Field-induced formation of nanoscale menisci. *Langmuir* 2008, 24, 6116–6120.
- (30) Wei, Z.; Zhao, Y. P. Growth of liquid bridge in AFM. J. Phys. D: Appl. Phys. 2007, 40, 4368.
- (31) Boinovich, L.; Emelyanenko, A. The prediction of wettability of curved surfaces on the basis of the isotherms of the disjoining pressure. *Colloids Surf.*, A 2011, 383, 10–16.
- (32) Raj, R.; Maroo, S. C.; Wang, E. N. Wettability of graphene. *Nano Lett.* 2013, 13, 1509—1515.
- (33) Kurra, N.; Scott, A.; Kulkarni, G. U. Electrocondensation and evaporation of attoliter water droplets: Direct visualization using atomic force microscopy. *Nano Res.* 2010, 3, 307–316.
- (34) Verdaguer, A.; Weis, C.; Oncins, G.; Ketteler, G.; Bluhm, H.; Salmeron, M. Growth and structure of water on SiO2 Films on Si investigated by kelvin probe microscopy and in situ x-ray spectroscopies. *Langmuir* 2007, 23, 9699–9703.
- (35) Xu, K.; Cao, P.; Heath, J. R. Graphene visualizes the first water adlayers on mica at ambient conditions. *Science* **2010**, 329, 1188–1191.
- (36) Dollekamp, E.; Bampoulis, P.; Faasen, D. P.; Zandvliet, H. J. W.; Kooij, E. S. Charge Induced Dynamics of Water in a Graphene–Mica Slit Pore. *Langmuir* 2017, 33, 11977–11985.
- (37) Komurasaki, H.; Tsukamoto, T.; Yamazaki, K.; Ogino, T. Layered structures of interfacial water and their effects on Raman spectra in graphene-on-sapphire systems. *J. Phys. Chem. C* 2012, 116, 10084–10089.
- (38) Lee, M. J.; Choi, J. S.; Kim, J.-S.; Byun, I.-S.; Lee, D. H.; Ryu, S.; Lee, C.; Park, B. H. Characteristics and effects of diffused water between graphene and a SiO<sub>2</sub> substrate. *Nano Res.* 2012, 5, 710–717.
- (39) Iler, R. K. The Chemistry of Silica: Solubility, Polymerization, Colloid and Surface Properties and Biochemistry of Silica; Wiley: New York, 1979.
- (40) Landfester, K.; Antonietti, M. Miniemulsions for the convenient synthesis of organic and inorganic nanoparticles and "single molecule" applications in materials chemistry. In *Colloids and Colloid Assemblies: Synthesis, Modification, Organization and Utilization of Colloid Particles*; Caruso, F., Ed.; John Wiley & Sons: Weinheim, Germany, 2003.

(41) Butt, H. J.; Untch, M. B.; Golriz, A.; Pihan, S. A.; Berger, R. Electric-field-induced condensation: An extension of the Kelvin equation. *Phys. Rev. E* 2011, 83, No. 061604.